Supplementary Information (SI) for Journal of Materials Chemistry A.
This journal is © The Royal Society of Chemistry 2026

Supplementary Information

In-Cell Electropolymerization of 10-(*N*-Pyrrolyl)phenoxazine into a Phenoxazine-Grafted Polypyrrole Cathode for High-Voltage and Ultrastable Li-Ion Batteries

Benhai Liu, [a] Jie Yi, [a] Cairong Shi, [a] Haishen Yang, [b] and Ya Du *[a]

[a] *B. Liu, J. Yi, C Shi, Prof. Y. Du*

School of Chemistry and Molecular Engineering, Institute of Advanced Synthesis, Nanjing Tech University, Nanjing 211816 Jiangsu, P. R. China

[b] *Prof. H. Yang*

Shanghai Key Laboratory of Materials Protection and Advanced Materials in Electric Power, College of Environmental and Chemical Engineering, Shanghai University of Electric Power, Shanghai, 200090, P. R. China

E-mail: ias_ydu@njtech.edu.cn.

Table of Contents

I. Methods

^{1}H spectra were recorded in $CDCl_3$ or DMSO-d_6 on Bruker Advance or Joel 400 MHz spectrometers. Fourier-transform infrared (FTIR) measurements were carried out with a Thermo Nicolet iS8 spectrometer. Powder X-ray diffraction (PXRD) patterns were recorded on a Smart Lab 3Kw (Rigaku Corporation). Thermal stability was evaluated by thermogravimetric analysis (TGA) using a METTLER TOLEDO TGA 2 system under a nitrogen atmosphere at a heating rate of 10 °C·min^{-1}. Sample morphology and microstructure were examined using a high-resolution cold field-emission scanning electron microscope (SEM, FEI Quanta FEG 250) equipped with energy-dispersive X-ray spectroscopy (EDS) for compositional analysis. Chemical composition analysis of both pristine and cycled electrodes was performed via ultraviolet-visible spectroscopy (UV-vis, PerkinElmer LAMBDA 950) and X-ray photoelectron spectroscopy (XPS, Thermo Scientific K‑Alpha, USA).

II. Materials Preparation

2.1 Materials

All chemicals and solvents were used as received unless otherwise specified. Solvents labeled as “anhydrous” were purchased and used directly; other solvents were purified by standard drying and distillation methods prior to use. Phenoxazine (98 wt.%), 1-Fluoro-4-nitrobenzene (98 wt.%), potassium hydroxide (KOH, 85 wt.%), tetrahydrofuran (THF, 98 wt.%), sodium acetate (CH_3COONa, 98 wt.%), sodium chloride (NaCl, 99.5 wt.%) were purchased from Aladdin. *N*, *N*-dimethylformamide (DMF, 99.5 wt.%), ethanol (EtOH, 99.7 wt.%), methanol (CH_3OH, 99.5 wt.%), sodium sulfate (Na_2SO_4, 99 wt.%) were supplied by China National Medicines Corporation Ltd. Ethyl acetate (EA, 99.5 wt.%), 2,5-Dimethyltetrahydrofuran ($C_6H_{12}O$, 98 wt.%) were obtained from Energy Chemistry. Hydrochloric acid (HCl, 37 wt.%), acetic acid (CH_3COOH, 99.5 wt.%), petroleum ether (PE, AR), dichloromethane (DCM, AR), trichloromethane ($CHCl_3$, AR) were purchased from Shanghai Lingfeng Chemical

Reagent Co., Ltd. Ferric chloride ($FeCl_3$, 99 wt.%) was obtained from Macklin. Dimethyl sulfoxide (DMSO, 99 wt.%) was supplied by General Reagent. N-Methylpyrrolidone (NMP, 99.5 wt.%) was purchased from Meryer.

2.2 Synthesis of the Monomer and Polymer

2.2.1 Synthesis of 10-(4-(1H-pyrrol-1-yl)phenyl)-10H-phenoxazine (4-PyPOZ)

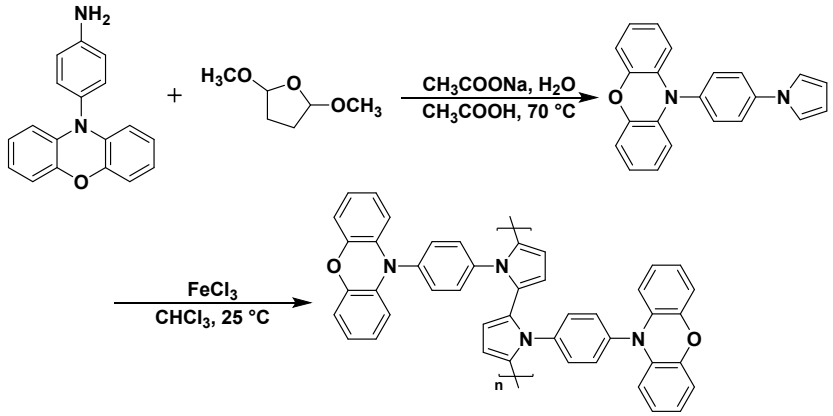

Scheme S1. Synthetic route of 10-(4-(1H-pyrrol-1-yl)phenyl)-10*H*-phenothiazine (4-PyPOZ) and ex-PPyPOZ.

Synthesis of 4-PyPOZ[1]: Sodium acetate (10 mmol, 0.82 g) was dissolved in water (40 mL) at room temperature, and the resulting solution was transferred to a round-bottom flask. Under a nitrogen atmosphere, the amine compound (10.3 mmol, 2.82 g) and glacial acetic acid (10 mL) were added sequentially. The mixture was stirred at 75 °C for 10 min. Subsequently, 2,5-dimethoxytetrahydrofuran (DMT) (20.6 mmol, 2.72 g) was added dropwise under vigorous stirring, and the reaction was maintained at 70 °C for 2.5 h. After cooling to room temperature, the mixture was extracted with dichloromethane (3×50 mL). The organic phase was washed with brine, dried over anhydrous Na_2SO_4, and concentrated under reduced pressure. The crude product was purified by silica gel column chromatography using a gradient mixture of dichloromethane and petroleum ether as eluent. ^{1}H NMR (400 MHz, DMSO-d_6) δ 7.87 (d, *J* = 8.8 Hz, 1H), 7.49 (dd, *J* = 5.2, 2.8 Hz, 2H), 6.76-6.73 (m, 1H), 6.69-6.65 (m, 2H), 6.32 (t, *J* = 2.2 Hz, 1H), 5.94-5.90 (m, 1H). ^{13}C NMR (101 MHz, DMSO-d_6) δ 143.1, 139.8,

135.0, 133.9, 131.8, 123.8, 121.8, 121.5, 119.1, 115.3, 113.2, 111.0. [M+ H], (m/ z, calc mass 325.1341, Found: 325.1337).

2.2.2 Synthesis of ex-PPyPOZ

Anhydrous $FeCl_3$ (4 mmol, 0.65 g) was placed in a round-bottom flask under a nitrogen atmosphere.[2] Anhydrous chloroform (7.5 mL) was added, and the mixture was sonicated for 5 min to afford a homogeneous solution. In a separate vessel, 4-PyPOZ (1 mmol, 0.324 g) was dissolved in anhydrous chloroform (11.5 mL). This solution was then added to the $FeCl_3$ solution under a nitrogen atmosphere. The resulting mixture was stirred at room temperature for 72 h. Upon completion, the reaction mixture was poured into vigorously stirred methanol (50 mL) to precipitate the product. The precipitate was collected by vacuum filtration and washed sequentially with water, 1 M HCl, and methanol, and dried in a vacuum oven at 90 °C for 12 h to give a gray powder (0.19 g, 50%).

III. Fabrication, Characterization and Electrochemical Measurements of Coin Cells

3.1 Preparation of Electrode

Coin-Type Cell Fabrication and Electrochemical Measurements.[3] The working electrode was prepared by mixing 60 wt.% 4-PyPOZ active material, 30 wt.% Ketjen Black (KB), and 10 wt.% poly(vinylidene fluoride) (PVDF) binder. The resulting slurry was blade-coated onto carbon-coated aluminum foil and dried at 80 °C under vacuum for 12 h. The mass loading of the active material was approximately 1.0 mg cm^{-2}. The electrode thickness was 250 μm, and the electrode area was 2 cm^2. CR2016 Coin cells were assembled in an argon-filled glovebox using lithium metal as the counter electrode, a Celgard 2400 polypropylene separator, and an electrolyte consisting of 1 M $LiPF_6$ in a mixture of ethylene carbonate, diethyl carbonate, and dimethyl carbonate (EC/DEC/DMC, 1:1:1 by volume). Galvanostatic charge/discharge tests were conducted on a NEWARE CT-4008 battery testing system. Electrochemical

measurements, including cyclic voltammetry (CV) at various scan rates within a voltage window of 1.5-4.5 V, and electrochemical impedance spectroscopy (EIS) over a frequency range of 10^6 to 10^{-2} Hz with a 5 mV amplitude, were performed on a CHI604E electrochemical workstation.

3.2 Preparation of Electrode Samples for X-ray and IR Characterization

For ex situ Fourier-transform infrared spectroscopy (FTIR) and X-ray photoelectron spectroscopy (XPS) measurements, Electrodes were prepared by homogenously mixing 4-PyPOZ, Ketjen Black (KB), and poly(vinylidene fluoride) (PVDF) binder in a mass ratio of 6:3:1. To characterize the cycled electrodes, the cells were carefully disassembled in an argon-filled glove box. The cycled electrodes were processed as follows.[4] The retrieved electrodes were immersed in 5 mL of diethyl carbonate (DEC) for 5 minutes to remove residual electrolytes; this rinsing step was repeated three times, each time with 5 mL of fresh DEC. Following the washing procedure, the electrodes were dried under vacuum at 80 °C. For scanning electron microscopy (SEM) imaging at various cutoff voltages, the electrodes were fabricated with a composition of 60 wt.% 4-PyPOZ powder, 30 wt.% carbon nanotubes, and 10 wt.% PVDF binder.

3.3 GPC Sample Preparation and Measurement Procedure

Sample Pretreatment: After electropolymerization and cycling, the PPyPOZ cathode was retrieved from the cell, rinsed thoroughly with dimethyl carbonate (DMC) to remove residual electrolyte, and dried under vacuum. The polymer material was then carefully scraped from the carbon-coated aluminum current collector. The collected powder was dissolved in HPLC-grade tetrahydrofuran (THF) at a concentration of approximately 2 mg mL^{-1} and stirred gently overnight to ensure complete dissolution. Prior to injection, the solution was filtered through a 0.22 μm PTFE syringe filter to remove any insoluble particulates.

GPC Measurement: GPC analysis was performed on a Waters 2414 system equipped with a refractive index (RI) detector. The mobile phase was HPLC-grade THF, maintained at a flow rate of 1.0 mL min^{-1} and a column temperature of 30 °C. Calibration was carried out using a series of polystyrene (PS) standards with narrow molecular weight distributions. A sample volume of 20 µL was injected for each measurement.

3.4 Defining the b-value in Pseudocapacitance

The charge storage mechanism of the electrode material was investigated by cyclic voltammetry (CV) at various scan rates. The relationship between the peak current (i) and the scan rate (v) follows a power law: $i = av^b$, where a is a constant and the b-value is a critical parameter for distinguishing the charge storage kinetics.[5] The b-value is obtained by linear fitting of the log(i) vs. log(v) plot. The b-value provides insight into the rate-limiting step: when the b-value exceeds 1.0, it suggests strong surface adsorption effects or super capacitive behavior, where kinetics are governed by surface charge transfer rather than bulk diffusion. A b-value close to 1.0 indicates a surface-controlled process (rate-independent kinetics), where current is proportional to scan rate. This is characteristic of ideal capacitive behavior, including both electric double-layer capacitors (EDLC) and fast surface redox reactions (pseudocapacitance). A b-value close to 0.5 reflects a semi-infinite linear diffusion-controlled process (bulk battery-like behavior), as described by the Randles-Sevcik equation. A b-value between 0.5 and 1.0 suggests a mixed kinetic process, where the charge storage is influenced by both diffusion and surface effects. This is often, but not exclusively, associated with pseudocapacitive materials that store charge via Faradaic reactions at or near the surface but may still have diffusion limitations depending on the electrode architecture.

3.5 Calculation and Analysis of Diffusion Coefficient Based on GITT

The galvanostatic intermittent titration technique (GITT) is a crucial electrochemical method employed to evaluate the kinetics of lithium-ion diffusion within electrode materials.[6] It is particularly useful for determining the chemical diffusion coefficient of Li^+ (D_{Li}^+) as a function of the state of charge (SOC). The measurement involves applying a series of constant current pulses to the cell for a limited time interval (τ), followed by a prolonged relaxation period to allow the cell voltage to return to its quasi-equilibrium state. By analyzing the transient voltage responses during both the current flux and the relaxation, the overpotential and the diffusion coefficient can be calculated. Based on Fick's second law of diffusion and the simplified Weppner & Huggins formula, the lithium-ion diffusion coefficient can be derived from the GITT potential profile:

$$D^{GITT} = \frac{4}{\pi\tau}\left(\frac{m_B V_m}{M_B S}\right)^2\left(\frac{\Delta E_s}{\Delta E_t}\right)^2 \left(t \leq \frac{L^2}{D}\right)$$

Where τ is the duration of the current pulse, M_B is the number of moles, V_M is the molar volume of the electrode material, M_B represents the molar mass of the active material, S is the electrode/electrolyte contact area, ΔE_s is the steady-state voltage change between two consecutive relaxation steps, and ΔE_t is the transient voltage change during the current pulse (after eliminating the iR drop). This analysis provides valuable insight into the rate-limiting steps and structural evolution during lithiation/delithiation**.**

IV. NMR Spectra and Figures

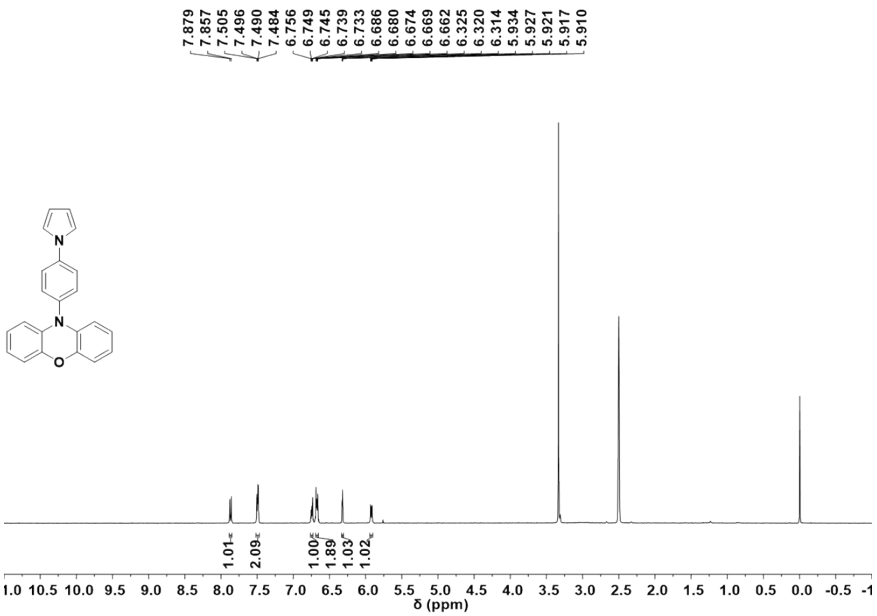

Figure S1. ^{1}H NMR spectrum (DMSO-d_6, 400 MHz) of 4-PyPOZ.

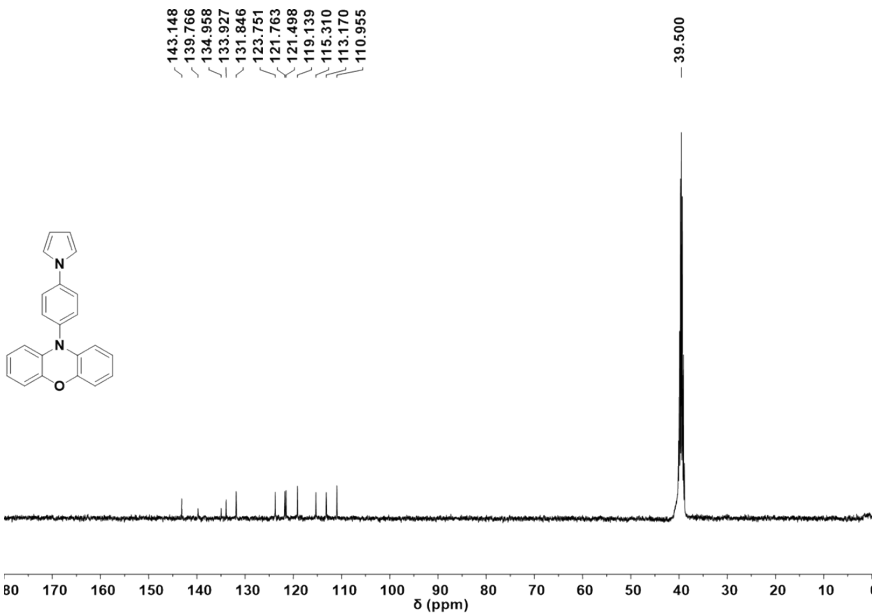

Figure S2. ^{13}C NMR spectrum (DMSO-d_6, 101 MHz) of 4-PyPOZ.

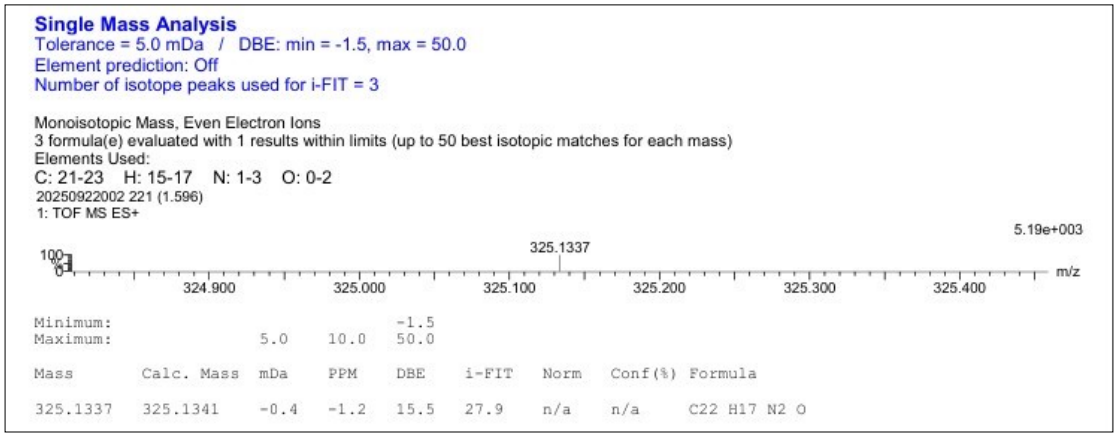

Figure S3. Mass spectrum of 4-PyPOZ.

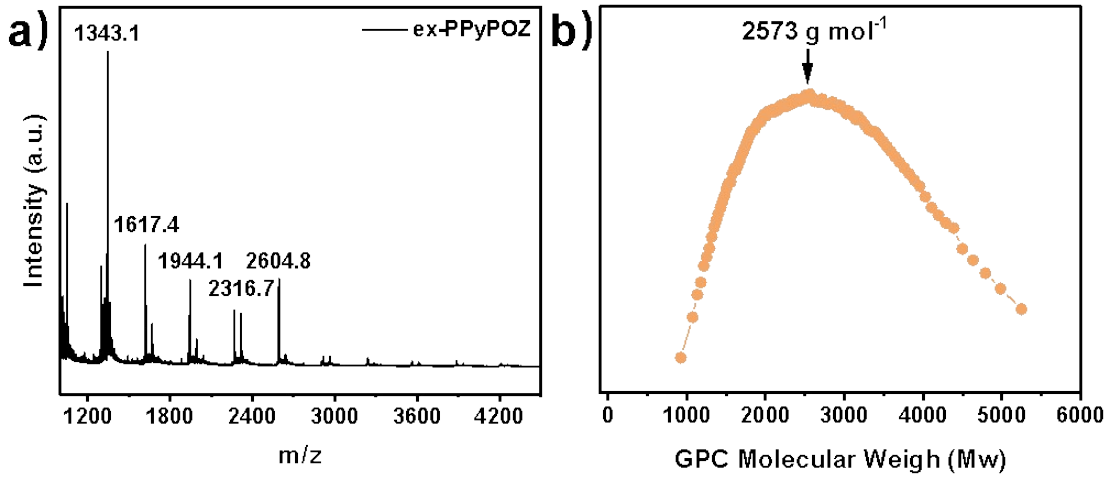

Figure S4. (a) MALDI-TOF mass spectrum and (b) GPC molecular weight distribution curve of ex-PPyPOZ.

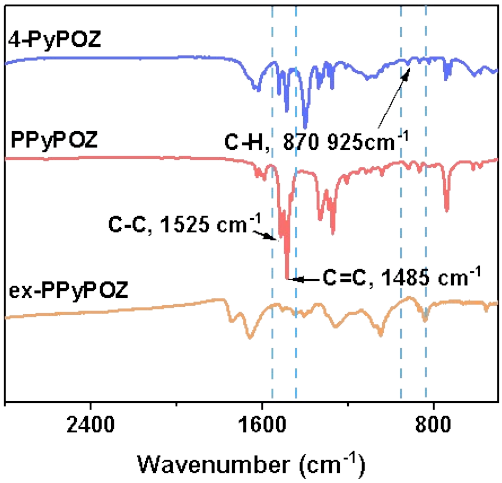

Figure S5. FTIR spectra of 4-PyPOZ, PPyPOZ and ex-PPyPOZ.

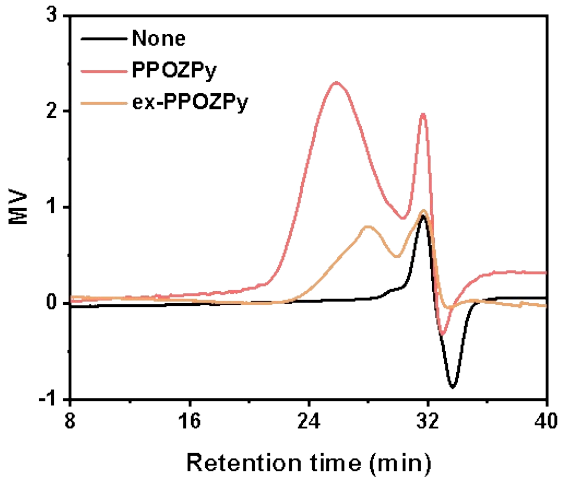

Figure S6. GPC elution traces of none, PPyPOZ and ex-PPyPOZ.

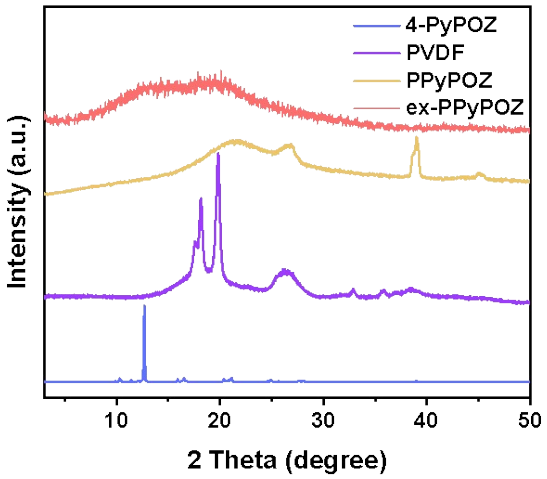

Figure S7. XRD spectrum of 4-PyPOZ, PVDF, PPyPOZ and ex-PPyPOZ.

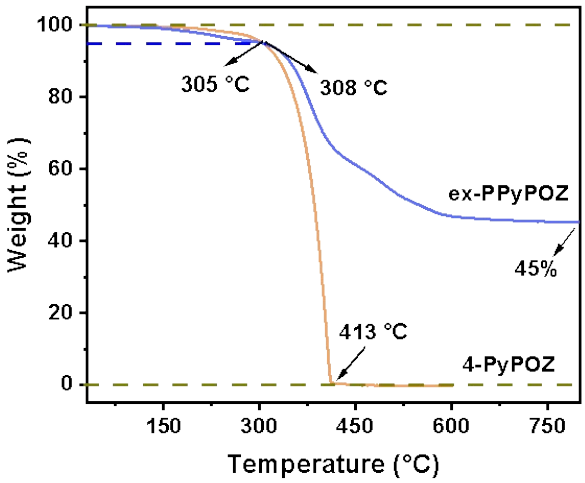

Figure S8. TGA results of 4-PyPOZ and ex-PPyPOZ.

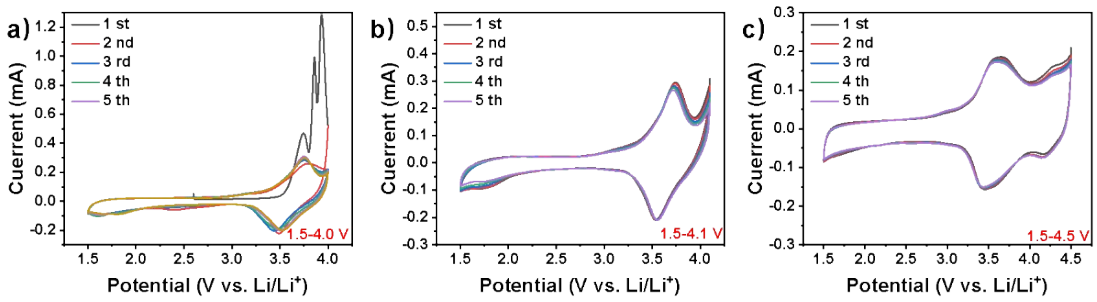

Figure S9. CV curves of PPyPOZ cathodes at different voltage ranges of (a) 1.5-4.0 V, (b) 1.5-4.1 V and (c) 1.5-4.5 V vs. Li/Li^+ at a scan rate of 1.0 mV s^{-1} in coin cells.

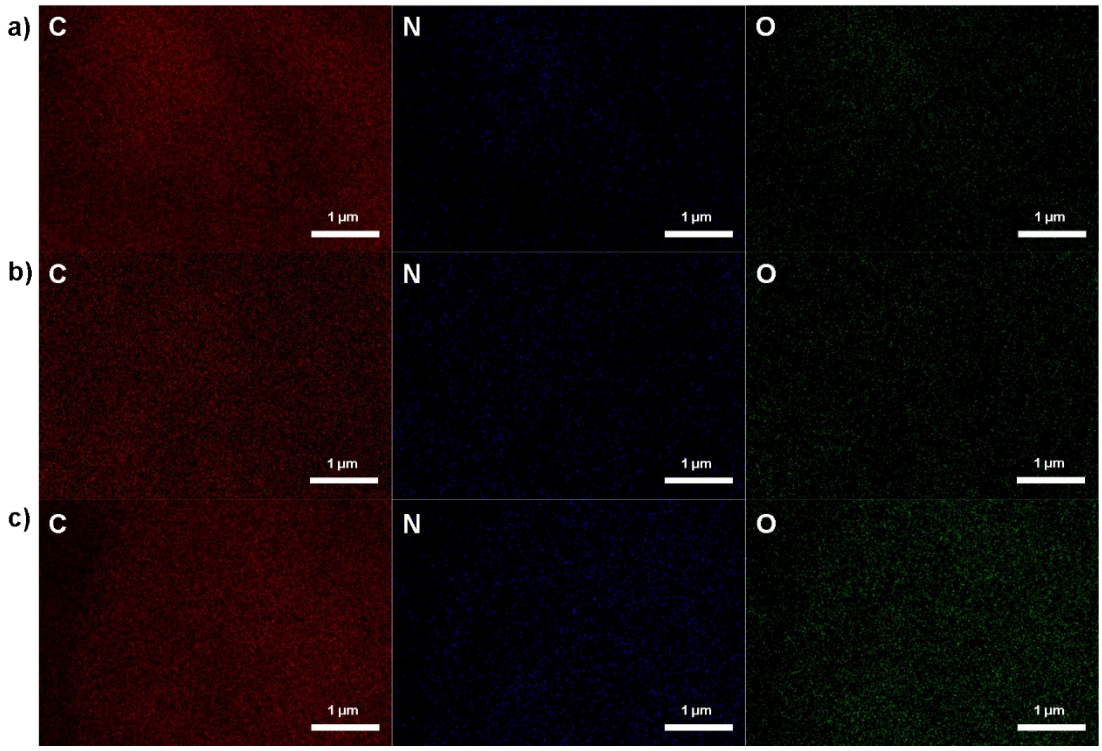

Figure S10. EDS elemental mapping of (a) the pristine electrode, (b) the electrode after low-voltage cycling, and (c) the electrode after high-voltage cycling.

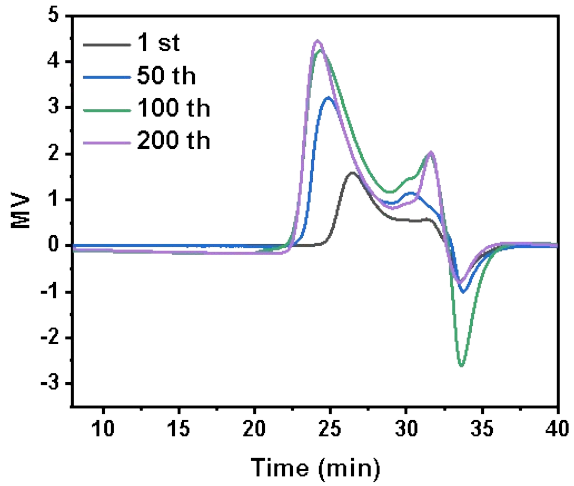

Figure S11. GPC elution traces of the PPyPOZ electrodes harvested after 1, 50, 100, and 200 cycles.

Table S1 GPC molecular weight data at varied cycle numbers.

Cycle number	Mn	Mw	PDI
1 st	3634	4431	1.219
50 th	6923	9719	1.404
100 th	7719	12076	1.646
200 th	8409	12724	1.513

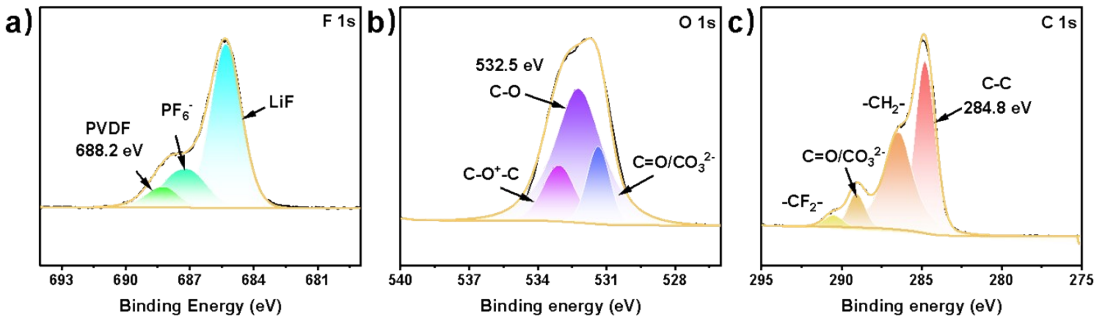

Figure S12 Ex situ XPS spectra of the PPyPOZ electrode cycled within 1.5-4.7 V: (a) F 1s, (b) O 1s, and (c) C 1s.

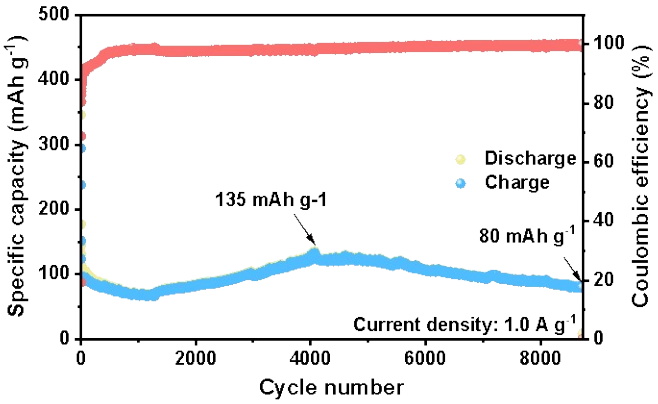

Figure S13. Long-term cycling performance of the PPyPOZ cathode at 1 A g^{-1}.

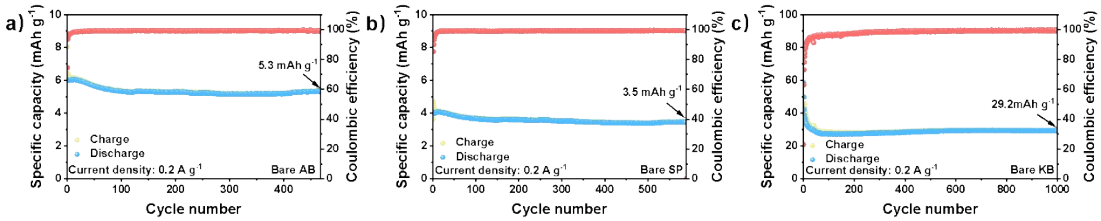

Figure S14. Cycling performance of (a) Acetylene black electrode, (b) Super P electrode and (c) Ketjen Black electrode at 0.2 A g^{-1} in 1.5-4.5 V.

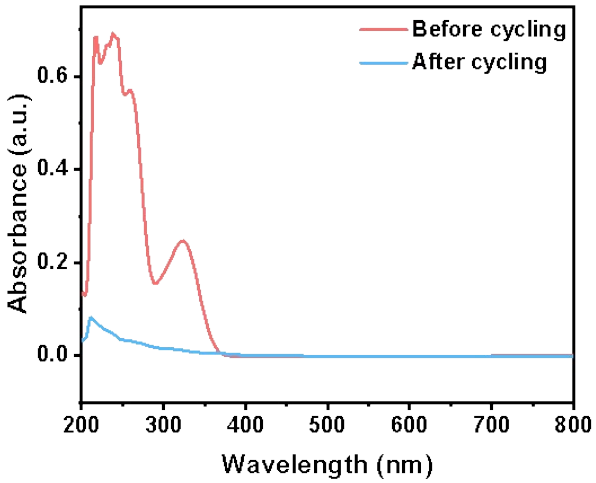

Figure S15. UV-vis absorption spectra of compound 4-PyPOZ and of the electrolyte solution in which the cycled PPyPOZ electrodes were soaked.

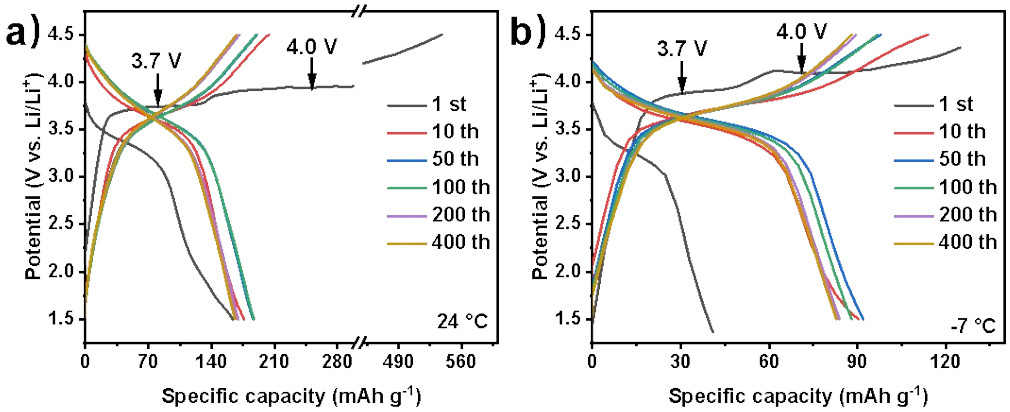

Figure S16. Galvanostatic charge/discharge curves of the PPyPOZ cathode at high mass loading (> 2 mg cm^{-2}) at (a) 24 °C and (b) -7 °C.

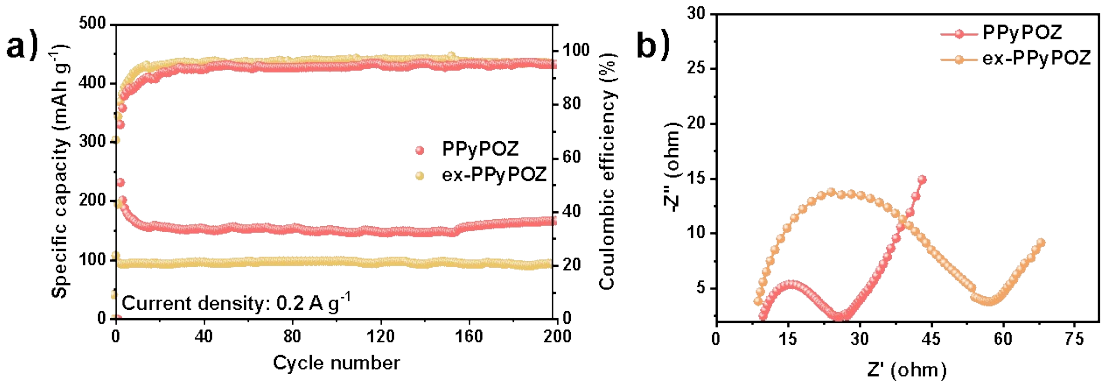

Figure S17. (a) Cycling stabilities of PPyPOZ and ex-PPyPOZ electrodes at 0.2 A g^{-1} in 1.5-4.5 V; (b) Nyquist plots of PPyPOZ and ex-PPyPOZ cathodes.

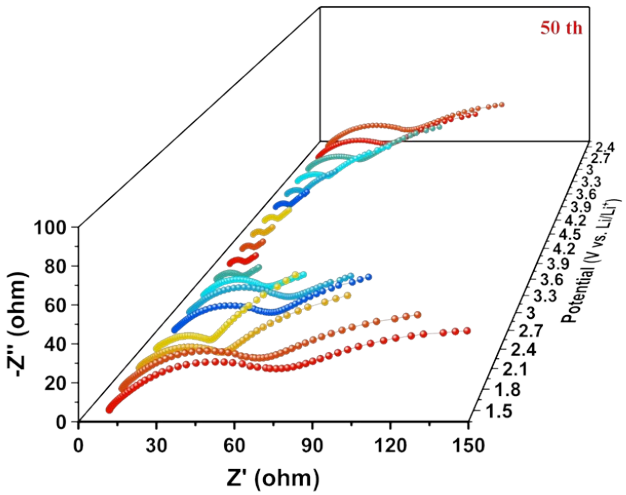

Figure S18. In situ EIS profiles of PPyPOZ cathode at the 50th cycles.

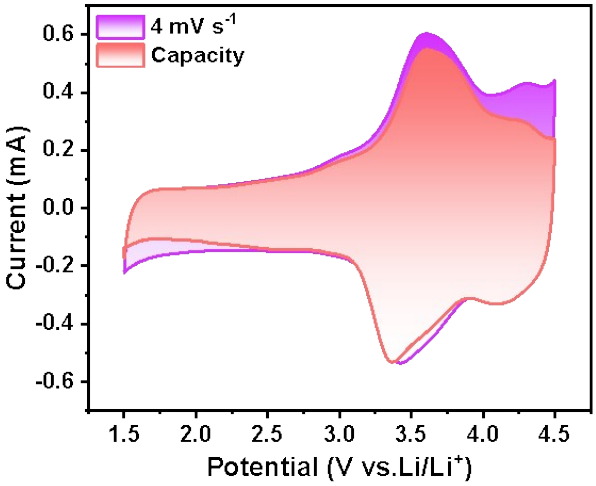

Figure S19. Capacitive contribution analysis for the PPyPOZ cathode at 4 mV s^{-1}.

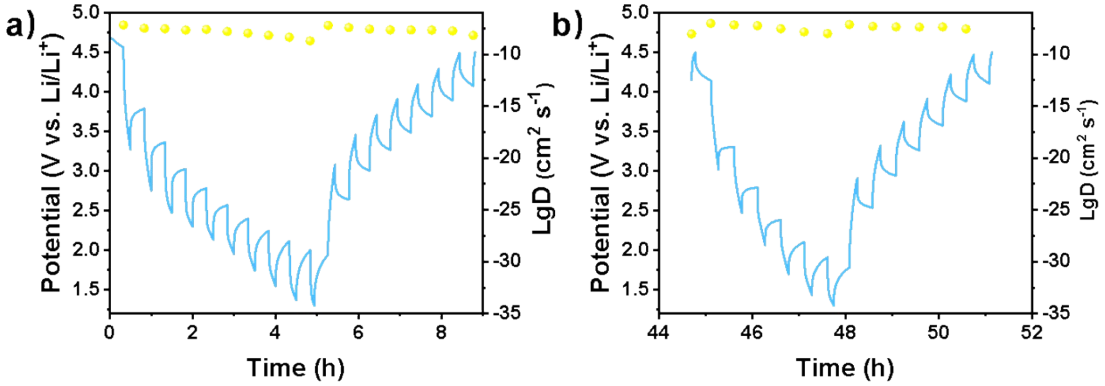

Figure S20. GITT curves and the calculated diffusion coefficients of charge/discharge processes for PPyPOZ cathodes, (a) 0-9 h and (b) 44-52 h.

V. Theoretical Calculations

All computational tasks were performed using Gaussian 09W. Geometry optimizations were conducted at the B3LYP-6-31G (d, p)* level.[7] Frequency calculations were performed at the same level to confirm that the obtained stationary points corresponded to true minima (no imaginary frequencies).[8, 9] The free energy values discussed in the manuscript are reported in kcal mol^{-1}. Electron density difference analysis and interaction region indicator (IRI) analysis for the 4-PyPOZ,[10] 4-PyPOZ-PF_6^- and 4-PyPOZ-$2PF_6^-$ systems were carried out using the Multiwfn program, with visualization conducted in VMD.[11]

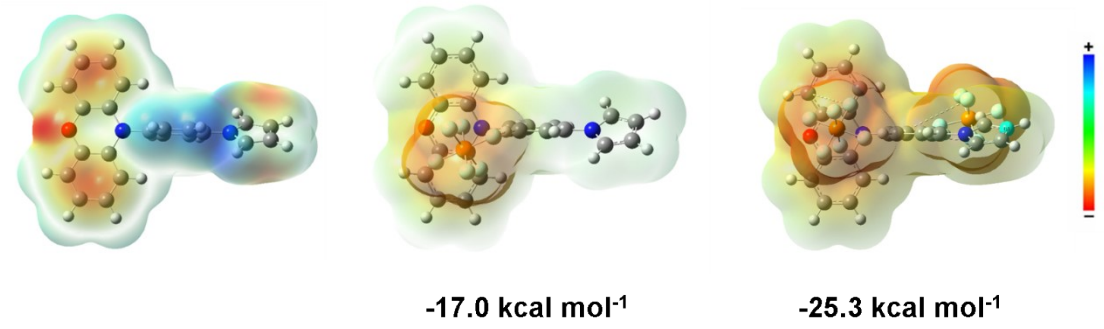

Figure S21. Electrostatic potential distributions for 4-PyPOZ at different cycled states.

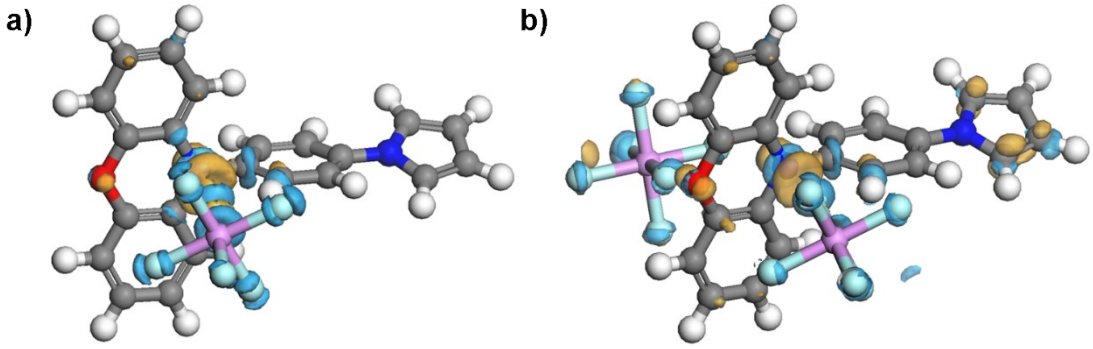

Figure S22. Charge density difference (CDD) analysis of 4-PyPOZ interacting with (a) one PF_6^- and (b) two PF_6^- anions.

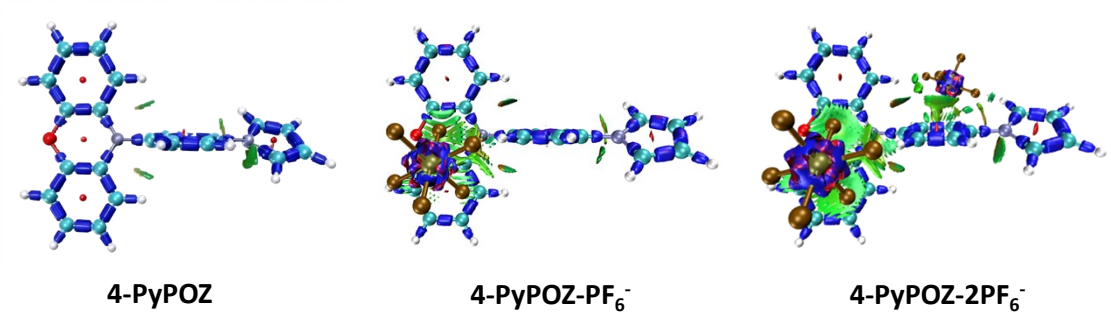

Figure S23. The interaction region indicator (IRI) analysis of 4-PyPOZ at different cycled states.

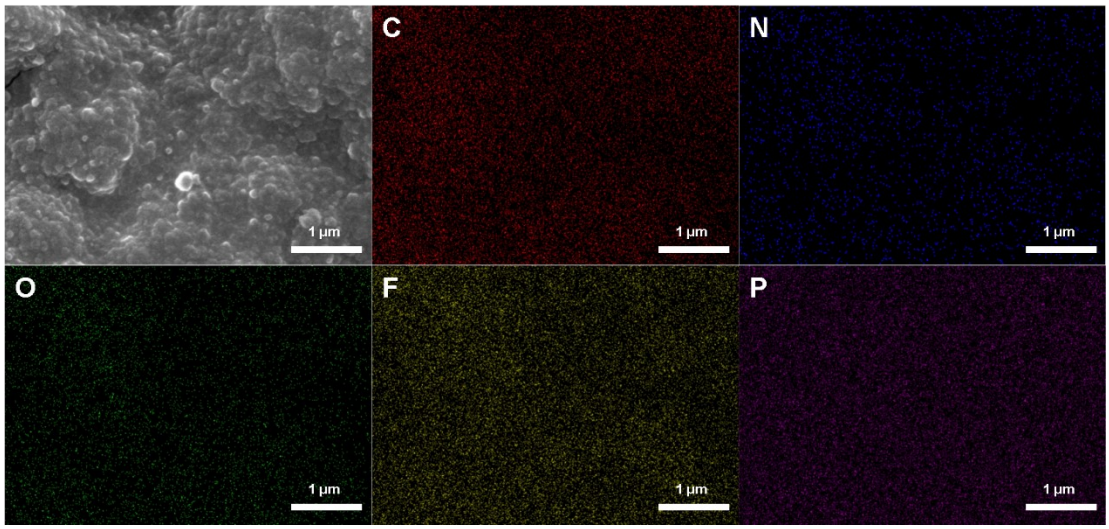

Figure S24. Ex situ EDS elemental mapping of the electrode after charging to 4.5 V, showing the elemental distributions of C, N, O, F, and P.

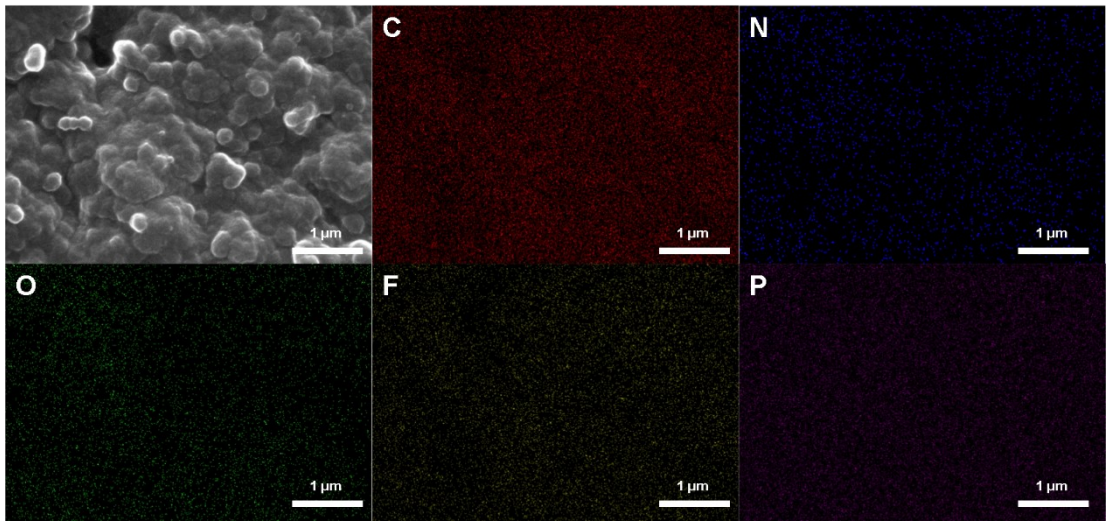

Figure S25. Ex situ EDS elemental mapping of the electrode after discharging to 1.5 V, showing the elemental distributions of C, N, O, F, and P.

Table S2. EDS semi-quantification of F, P, and F/P ratios in charged and discharged states.

State	F (wt%)	P (wt%)	F (atom%)	P (atom%)	F/P atomic ratio
Charged	17.35	2.29	12.37	1.84	6.72
Discharged	5.68	1.79	3.87	0.75	5.20

Table S3. Performance comparison of representative high-voltage organic cathodes.

Material	Voltage (V)	Capacity (mAh g^{-1})	Energy density (Wh kg^{-1})	Cycle life	Current density (A g^{-1})	Ref.
PPT-DHP	3.61	129.2	502.1	-	0.1	[12]
PQ	2.74	248	679.5	100	-	[13]
TTF-COFs	3.6	47.5	171	400	-	[14]
DNP-Li	3.55	140	497	50	-	[15]
PHX	3.5	181.3	600	-	-	[16]
CuCA	2.8	165.5	463.4	50	0.5	[17]
PPTO-2PH	2.9	372	1078.8	1100	0.2	[18]
TCTA	3.95	48	189.6	5000	1	[19]
Poly$(FeL)_n$	2.02	113.9	550	4000	5	[20]
Cu(TCNQ)	4.26	106.2	947	200	5	[21]
TPPDA-CuPor-COF	2.7	104	371	3000	1	[22]
POFP	3.6	69	248.4	500	0.2	[23]
IEP-29	3.6	95	342	2000	-	[24]
PIBT-1	4.0	62	248	100	0.05	[25]
p-TP4OLi	2.4	195	468	100	0.05	[26]
PPyPOZ	3.6	174	626.4	1200	0.2	*This work*

VI. References

1. L. Xu, P. Guo, H. He, N. Zhou, J. Ma, G. Wang, C. Zhang and C. Su, *Ionics*, 2017, **23**, 1375-1382
2. L. Xu, S. Zhang, P. Guo and C. Su, *ChemistrySelect*, 2021, **6**, 4725-4735
3. J. Y. Cao, F. F. Ding, H. P. Chen, H. N. Wang, W. C. Wang, Z. D. Chen and J. Xu, *J. Power Sources*, 2019, **423**, 316-322.

4. X. H. Wang, X. Y. Kong, J. W. Wang, Y. L. Lin, H. M. Sun and W. W. Huang, *ACS Sustainable Chem. Eng.*, 2022, **10**, 15760-15766.
5. S. E. Bak, W. Chung, M. A. Abbas and J. H. Bang, *ACS Appl. Energy Mater.*, 2022, **5**, 5508-5512.
6. H. A. A. Ali, L. H. J. Raijmakers, A. Windmüller, H. Tempel, B. Liaw, P. H. L. Notten and R. A. Eichel, *J. Energy Storage*, 2025, **132**, 11768
7. A. Suvilal, A. B. Krishna, R. Vamadevan and J. S. Babu, *J. Energy Storage*, 2026, **141**, 19465.
8. Y. Qian, S. Jiang, Y. Li, Z. Yi, J. Zhou, T. Q. Li, Y. Han, Y. S. Wang, J. Tian, N. Lin and Y. T. Qian, *Adv. Energy Mater.*, 2019, **9**, 1901676.
9. Z. H. Yang, X. B. Huang, P. Y. Meng, M. Jiang, Y. B. Wang, Z. P. Yao, J. Zhang, B. D. Sun and C. P. Fu, *Angew. Chem. Int. Ed.*, 2023, **62**, e202216797.
10. J. J. Wang, B. Lin, P. Wang, L. Q. Tao, Y. Zhang and S. Q. Li, *J. Environ. Chem. Eng.*, 2024, **12**, 112550.
11. T. Lu and F. W. Chen, *J. Comput. Chem.*, 2012, **33**, 580-592.
12. Q. S. Bai, K. Huang, X. Y. Wu and Y. L. Zhu, *Chin. J. Chem.*, 2025, **43**, 3561-3568.
13. Y. J. Gao, J. M. Fu, Y. Hu, F. P. Zhao, W. H. Li, S. X. Deng, Y. P. Sun, X. G. Hao, J. J. Ma, X. T. Lin, C. H. Wang, R. Y. Li and X. L. Sun, *Angew. Chem. Int. Ed.*, 2024, **63**, e202403331.
14. G. Valente, R. Dantas, P. Ferreira, R. Grieco, N. Patil, A. Guillem-Navajas, D. R. S. Miguel, F. Zamora, R. Guntermann, T. Bein, J. Rocha, M. H. Braga, K. Strutynski, M. Melle-Franco, R. Marcilla and M. Souto, *J. Mater. Chem. A*, 2024, **12**, 24156-24164.
15. A. E. Lakraychi, I. E. Udom, W. Ren and Y. Yao, *ChemSusChem*, 2025, **18**, e202402779.
16. M. Sun, S. Liu, P. Leung, X. Y. Wan, L. J. Li, Z. H. Zhang, F. C. Walsh, R. A. P. Camacho, L. Lu and Q. Liao, *Adv. Funct. Mater.*, 2026, **36**, e19300.
17. Y. W. Luo, J. L. Liu and L. Zhang, *Angew. Chem. Int. Ed.*, 2022, **61**, e202209458.

18. B. Ouyang, D. Huang, X. H. Bian, J. Y. Guo, X. L. Peng, Y. Du and H. S. Yang, *Chem. Eng. J.*, 2025, **508**, 161004.
19. C. Zhao, Z. F. Chen, W. Wang, P. X. Xiong, B. F. Li, M. J. Li, J. X. Yang and Y. H. Xu, *Angew. Chem. Int. Ed.*, 2020, **59**, 11992-11998.
20. C. X. Zhang, S. L. Mei, C. Cao, W. S. Zhang, X. H. Chen, T. F. He, Y. S. Feng, G. K. Long, G. Q. Tan, Y. W. Zhong and C. J. Yao, *Small*, 2025, **21**, 2503163.
21. H. D. Wang, Q. Wu, Y. N. Wang, X. L. Lv and H. G. Wang, *J. Colloid Interface Sci.*, 2022, **606**, 1024-1030.
22. L. Gong, X. Y. Yang, Y. Gao, G. X. Yang, Z. H. Yu, X. Z. Fu, Y. H. Wang, D. D. Qi, Y. Z. Bian, K. Wang and J. Z. Jiang, *J. Mater. Chem. A*, 2022, **10**, 16595-16601.
23. F. Otteny, V. Perner, D. Wassy, M. Kolek, P. Bieker, M. Winter and B. Esser, *ACS Sustainable Chem. Eng.*, 2020, **8**, 238-247.
24. H. Bildirir, D. Alván, N. Patil, V. A. D. O'Shea, M. Liras and R. Marcilla, *ACS Appl. Polym. Mater.*, 2023, **6**, 10092-10101.
25. A. L. Lubis, F. Baskoro, T. H. Lin, H. Q. Wong, G. S. Liou and H. J. Yen, *ACS Appl. Mater. Interfaces*, 2023, **16**, 48722-48735.
26. Q. H. Yu, W. Tang, Y. Hu, J. Gao, M. Wang, S. H. Liu, H. H. Lai, L. Xu and C. Fan, *Chem. Eng. J.*, 2021, **415**, 128509.